ORIGINAL PAPER



Identifying empirical equations of chaotic circuit from data

Artur Karimov · Vyacheslav Rybin · Ekaterina Kopets · Timur Karimov · Erivelton Nepomuceno · Denis Butusovo

Received: 16 May 2022 / Accepted: 24 August 2022 / Published online: 17 September 2022 © The Author(s), under exclusive licence to Springer Nature B.V. 2022

Abstract Chaotic analog circuits are commonly used to demonstrate the physical existence of chaotic systems and investigate the variety of possible applications. A notable disparity between the analog circuit and the computer model of a chaotic system is usually observed, caused by circuit element imperfectness and numerical errors in discrete simulation. In order to show that the major component of observable error originates from the circuit and to obtain its accurate white-box model, we propose a novel technique for reconstructing ordinary differential equations (ODEs) describing the circuit from data. To perform this task, a special system reconstruction algorithm based on iteratively reweighted least squares and a special synchronization-based technique for comparing model accuracy are developed. We investigate an example of a well-studied Rössler chaotic system. We implement the circuit using two types of operational amplifiers. Then, we reconstruct their ODEs from the recorded data. Finally, we compare original ODEs, SPICE models, and reconstructed equations showing that the reconstructed ODEs have approximately 100 times lower mean synchronization error than the original equations. The proposed identification technique can be applied to an arbitrary nonlinear circuit in order to obtain its accurate empirical model.

Keywords Chaos · Identification · Rossler circuit · Numerical simulation

Chaotic systems have been studied for several decades,

and multiple techniques were introduced for their anal-

ysis. One of the most known techniques is analog sim-

ulation via circuit implementation. It is known that ordinary differential equations (ODEs) describing the

chaotic system can be easily transformed into a circuit

with operational amplifiers, analog multipliers and pas-

sive electronic components [1,2]. An interest in chaotic

circuits raised significantly after L. Chua's work on the

Mathematics Subject Classification 93B30 · M34C28

1 Introduction

A. Karimov · V. Rybin · E. Kopets · T. Karimov · D. Butusov (\(\sigma \)

Youth Research Institute, ETU LETI, ul. Professora Popova 5, Saint Petersburg, Russian Federation 197022 e-mail: dnbutusov@etu.ru

A. Karimov

e-mail: aikarimov@etu.ru

V. Rybin

e-mail: vgrybin@etu.ru

E. Kopets

e-mail: eekopets@etu.ru

e-mail: tikarimov@etu.ru

E. Nepomuceno

Centre for Ocean Energy Research, Maynooth University, Maynooth, County Kildare, Ireland e-mail: erivelton.nepomuceno@mu.ie

Springer

circuit with double-scroll attractor [3] which was later elegantly extended by M. Kennedy [4]. To be exact, chaos had been observed in some earlier electronic circuits such as Van der Pol's oscillator, but this type of behavior was properly explained much later [5]. Nowadays, while powerful and precise digital computers are widespread, many studies on chaos still involve circuit realizations [6–12], both in simulators and in real hardware. It would not be an exaggeration to say that circuit implementation became a "golden standard" in scientific publications dedicated to chaotic systems.

Analog realization is often considered as a way of demonstrating the physical existence of chaotic systems and a sort of transition from theory to practice [13], but chaotic circuits themselves attract scholars and engineers as well. A number of studies are dedicated to creating efficient and precise electronic implementations of chaotic systems, including fractional-order systems and systems with memristors [14–22]. A plethora of possible applications of analog chaotic circuits is known: accurate sensing [23,24], measurement [2,25] and secure communication [26,27].

There are several reasons why high correspondence between the circuit and the model is important. From the theoretical point of view, it allows substantiating that the system is implemented correctly. On the other hand, in practice, it is a way to better operate the circuit by understanding the design flaws and resolving them. In real-life applications, the lack of accuracy of analog implementation is a bottleneck in the transition from the mathematical model to the circuit, especially when basic off-shelf electronic components are used.

The standard design procedure implies analog implementation as follows: First, an ODE of the chaotic system is obtained, and the desired properties are confirmed using numerical ODE solvers. After that, a SPICE model is designed and verified, and then a real circuit is prototyped and tested. The limited correspondence between the original ODE to be implemented and the circuit is clear: The chaotic differential equation does not take into account any implementation issues. But it is important to notice that the accuracy of a SPICE model in chaotic systems simulation is also controversial. The manufacturers often recommend verifying SPICE computer models [28], and there exists a proven problem with chaotic system simulation reproducibility [29]. One of the major reasons for SPICE models inaccuracy is that only simplified models of many complicated devices are available for SPICE simulation.

Examples of such devices are operational amplifiers and analog multipliers. Therefore, the accuracy of a real circuit implementation can be addressed mostly experimentally.

Another challenging question arises when considering the accuracy of the model. The problem is how to estimate the error between the original chaotic system and its analog implementation. One possible way here is to compare some metrics like bifurcation points [30]. Another approach is to synchronize a computer model of the system with the circuit, and the synchronization error will be proportional to distortions introduced by the circuit. The latter is true if the computer model is constructed using a high-order integration method, and the discretization time step is small enough [31]. Applying the last approach to the Rössler system revealed that besides parameter inaccuracy, discretization error and noise, there exists another source of error causing disparity between the circuit and the model, which has not been figured out exactly [31-34]. The main hypothesis of the current study is that these errors originate from unaccounted nonlinearities of analog integrated circuits. To estimate these nonlinearities, one should establish the white-box model which would accurately describe the dynamics of the circuit.

The current study aims at proposing a novel approach to reconstructing the mathematical model of an analog chaotic circuit and establishing a reliable way for its verification. The suggested procedure for obtaining an empirical ODE from the circuit is based on machine learning algorithms for nonlinear system identification, which have significantly advanced in the last decades [35–40]. Verification of the obtained ODE is performed via synchronization with real data following the improved procedure from [31].

The analog implementation of Rössler system was chosen for investigation. It is a canonical example of a chaotic attractor and has simple equations with single nonlinearity. It can be implemented in many ways; the most popular variant contains an analog multiplier [31, 33,41–43]. We compare two variants of the Rössler analog circuit with various operational amplifiers and AD633JN multiplier.

The rest of the paper is organized as follows. In Sect. 2, we describe numerical procedures of system identification and model error estimation. We also describe how the Rössler system is implemented in circuitry. Section 3 presents the experimental results. We



compare the geometrical properties of obtained attractors and estimate errors of conventional and empirical models. Section 4 gives discussion and conclusions.

2 Materials and methods

This section describes the theory behind the current study. First, we describe how data obtained from the circuit can be used for the mathematical model reconstruction in the form of a polynomial ODE. Then, we describe a technique for model accuracy estimation using chaotic synchronization. Finally, we consider a way how to implement the Rössler system as a circuit.

2.1 ODE reconstruction from data

Let us propose the method for ODE reconstruction using experimental data. Consider the initial value problem given by an ODE:

$$\dot{\mathbf{x}}(t) = \mathbf{f}(t, \mathbf{x}), \ \mathbf{x}(0) = \mathbf{x}_0, \tag{1}$$

where $\mathbf{x} = (x_1, x_2 \dots x_m)^{\top}$.

The problem of ODE reconstruction is finding the unknown function $\mathbf{f}(t, \mathbf{x})$ when n observations on the system are available. This problem is a special case of regression.

Suppose observations contain full information on system states $\mathbb{X} = \{\mathbf{x}_1, \mathbf{x}_2, \dots \mathbf{x}_n\}$ and their derivatives $\mathbb{Y} = \{\dot{\mathbf{x}}_1, \dot{\mathbf{x}}_2, \dots \dot{\mathbf{x}}_n\}$ at times $\mathbf{t} = \{t_1, t_2, \dots t_n\}$.

We look for the function $\mathbf{f}(t, \mathbf{x})$ in the form of a multivariate polynomial:

$$\mathbf{f}(t, \mathbf{x}) = \begin{pmatrix} \sum_{i=1}^{L_1} h_{1i} \tau_{1i}(t, \mathbf{x}) \\ \sum_{i=1}^{L_2} h_{2i} \tau_{2i}(t, \mathbf{x}) \\ \vdots \\ \sum_{i=1}^{L_m} h_{mi} \tau_{mi}(t, \mathbf{x}) \end{pmatrix}, \tag{2}$$

where m is the dimension of the system, $\tau_{ki}(t, \mathbf{x})$ is a monomial composed of variables at different powers, such as $x_1x_2^2x_3^2$, and h_{ki} is a scalar coefficient by the monomial. The overall number of monomials in kth entry is L_k .

Introduce a matrix of monomial values, calculated on a set X:

$$E_{k} = \begin{pmatrix} \tau_{k1}(t_{1}, \mathbf{x}_{1}) & \tau_{k2}(t_{1}, \mathbf{x}_{1}) & \dots & \tau_{kL_{k}}(t_{1}, \mathbf{x}_{1}) \\ \tau_{k1}(t_{2}, \mathbf{x}_{2}) & \tau_{k2}(t_{1}, \mathbf{x}_{2}) & \dots & \tau_{kL_{k}}(t_{1}, \mathbf{x}_{2}) \\ \vdots & \vdots & \ddots & \vdots \\ \tau_{k1}(t_{n}, \mathbf{x}_{n}) & \tau_{k2}(t_{n}, \mathbf{x}_{n}) & \dots & \tau_{kL_{k}}(t_{n}, \mathbf{x}_{n}) \end{pmatrix} . \quad (3)$$

The set of n derivatives of x_k can be considered as a vector:

$$\mathbf{y}_{k} = \begin{pmatrix} \dot{x}_{k}(t_{1}) \\ \dot{x}_{k}(t_{2}) \\ \vdots \\ \dot{x}_{k}(t_{n}) \end{pmatrix}, \tag{4}$$

and all coefficients by monomials in kth entry of (2) also make up a vector:

$$\mathbf{h}_{k} = \begin{pmatrix} h_{k1} \\ h_{k2} \\ \vdots \\ h_{kL} \end{pmatrix}. \tag{5}$$

Let us recall that each entry in the vector function (2) is a weighted sum of nonlinear monomials, and each of them is known. Therefore, since $\dot{x}_k(t) = f_k(t, \mathbf{x})$, the vector \mathbf{h}_k can be estimated as a solution of an overdetermined equation

$$\mathbf{y}_k = E_k \mathbf{h}_k. \tag{6}$$

The solution of (6) is found as follows:

$$\mathbf{h}_k = (E_k^{\top} E_k)^{-1} (E_k^{\top} \mathbf{y}_k). \tag{7}$$

This method for solving (6) is called ordinary least squares (OLS). In practice, due to noise, not all observations are equally useful for reconstructing the equation. Also, it is often preferred to set as many coefficients h_{ki} to zero as possible. Therefore, ℓ_1 -regularized iteratively reweighted least squares (IRLS) are preferred, which solves the following minimization problem using any applicable nonlinear optimization technique:

$$\mathbf{h}_k = \arg\min_{\mathbf{h}} \left(\sum_{i=1}^n w_i \| y_{ki} - E_{ki} \mathbf{h} \|^2 + \alpha |\mathbf{h}| \right),$$

where w_i are weights, initially set to ones, and α is the regularization parameter: Increasing α , one can set more coefficients h_{ki} to zero. The solution (7) is used as a starting point for optimization. On each iteration, weights are updated according to the formula

$$w_i = \frac{1}{\max(\delta, |y_{ki} - E_{ki}\mathbf{h}^j|)}, \ i = [1..n].$$
 (8)



The quantity δ is a relatively small number that limits w_i , preventing division by zero in (8). A more detailed description of IRLS can be found in [38].

Additional procedures are often needed to make the ODE reconstruction more stable and sparse. First, one should check whether any of the monomials τ_{ki} vanishes on data, i.e., it is not equal to zero in all sample points: $\{ \forall (t, \mathbf{x}) \in \mathbf{t} \times \mathbb{X} | \tau_{ki}(t, \mathbf{x}) = 0 \}$. If any of the monomials τ_{ki} is vanishing, the least squares problem becomes ill-posed and cannot be solved accurately. So, vanishing monomials should be eliminated.

To do this, in the presence of noise in data \mathbb{X} , an approximate Buchberger–Möller (ABM) algorithm can be used. It was first proposed in [44] and first applied to ODE reconstruction in [35], so we refer the reader to these works and omit its detailed description. Briefly, the idea of ABM algorithm is as follows. We iteratively add candidate monomials τ_{ki} into a feasible monomial set O. At each iteration, we estimate the matrix E_k (3), calculate the matrix $B_k = E_k^{\top} E_k$ and find its smallest eigenvalue λ_{\min} . If $\lambda_{\min} < \varepsilon$, where ε is a given threshold, the candidate monomial is rejected since it is likely to be vanishing; otherwise, it is added to the set O.

Some other methods for eliminating vanishing monomials are also known [45,46], but, in our opinion, they are more complicated and hard to implement than the ABM algorithm.

In order to reduce the number of monomials in the regression, we propose using a special procedure delMinorTerms, adopted from Kera and Hasegawa [35]. The idea of delMinorTerms is following: After estimating all entries of \mathbf{h}_k , an index i of a monomial $h_{ki}\tau_i(t,\mathbf{x})$ having the minimal norm on a set \mathbb{X} is determined and this monomial is excluded from the regression, while the remaining coefficients h_{ki} are found once again using least squares. In practice, ℓ_1 -regularization is not always necessary, and if it is used, small values of α give more stable results [35].

The overall proposed ODE reconstruction method is outlined in pseudocode in Algorithm 1. First, $deglexord(p_{min}, p_{max}, m)$ procedure is used to generate a set of degree-lexicographically ordered monomials σ of powers from p_{min} to p_{max} , previously described in the work [36]. Degree-lexicographic order is one of several possible monomial orders which implies that monomials are first graded by a total degree and then by the alphabetic order of variables constituting them [47]. For example, in case of a three-

dimensional system with variables x, y, z, degreelexicographic order for $p_{\min} = 0$ and $p_{\max} = 2$ is $\{1, x, y, z, x^2, xy, xz, y^2, yz, z^2\}$. Then, an approximate Buchberger-Möller algorithm is applied to obtain O – a set of nonvanishing monomials. After that, for each dimension k of the original system, initial approximation \mathbf{h}_k is found using (7). This value is a starting point for optimization in delMinorTerms procedure, which returns $\{h_{ki}\}$, $\{\tau_{ki}\}$ for the current k. Two tolerances are involved in the algorithm: ε is used in the ABM algorithm, and η controls minor term elimination in del Minor Terms procedure. For simplicity, t is not considered: It can be treated as an additional column in X in case the system is non-autonomous. The main difference between delMinorTerms variant used in our code and previously published ones [35–37] is that it uses IRLS instead of the other least squares. The most detailed description of the algorithm can be found in [35].

Algorithm 1: ODE reconstruction algorithm

```
Input: \mathbb{X}, \mathbb{Y}, \mathbf{t}.

Output: \{h_{ki}\}, \{\tau_{ki}\}, i = [1..L], k = [1..m].

Initialization:

\sigma \leftarrow deglexord(p_{\min}, p_{\max}, m); // obtain all possible monomials

O \leftarrow ABM(\mathbb{X}, \varepsilon, \sigma); // exclude vanishing monomials

for k = l \dots m do

\mathbf{h}_k = (E^\top E)^{-1}(E^\top \mathbf{y}_k); // initial approximation of \mathbf{h}_k

\{h_{ki}\}, \{\tau_{ki}\} \leftarrow
delMinorTerms(\mathbb{X}, \mathbb{Y}, O, \eta, \mathbf{h}_k, \alpha); // exclude minor monomials

end
```

Thus, the obtained model of the system is uniquely described by two sets $\{h_{ki}\}$, $\{\tau_{ki}\}$, $i=[1\dots L]$, $k=[1\dots m]$ used in (2) when solving the ODE. Finetuning of the parameters α and η can reduce the number of monomials in the model, in other words, improve sparsity. But usually, there is an unavoidable trade-off between accuracy and sparsity [48], and in general, if the solution should be as accurate as possible, sparsity should be sacrificed.



2.2 Model error estimation through synchronization

Once a dataset of system states $\mathbb{X} = \{\mathbf{x}_1, \mathbf{x}_2, \dots, \mathbf{x}_N\}$ and their derivatives $\mathbb{Y} = \{\dot{\mathbf{x}}_1, \dot{\mathbf{x}}_2, \dots, \dot{\mathbf{x}}_N\}$ at times $\mathbf{t} = \{t_1, t_2, \dots t_N\}$ is collected, and a model (2) is obtained, the model accuracy should be tested. For chaotic systems, a phenomenon of synchronization provides an attractive framework for solving the problem. It is known that trajectories of chaotic systems diverge exponentially in absence of any coupling between them, even if systems are similar. But, if a coupling is added, for example, in a form of a proportional feedback controller, chaotic systems exhibit correlated dynamics. Depending on the type of this correlation, there can be complete synchronization, lag synchronization, generalized synchronization, and so on [49]. The generalized synchronization is of special interest, because it may happen between different systems. For example, it is usually possible to synchronize analog and computer models of a chaotic flow, but due to the difference between these systems the synchronization is not complete but generalized.

In our previous work [31], we substantiated a conjecture that the error between the system trajectories vanishes if the discretization time step and the distance between the synchronized systems in function space tend to be zero; otherwise, there may exist a bounded chaotic attractor of error between system trajectories. The L_1 -volume of this attractor as well as its other parameters is proportional to the disparity of the systems to each other. So, after the transient in the synchronized computer model dies out, measuring the average error norm between trajectories of the circuit and the model provides a metric for the model accuracy estimation. This metric is more qualitative than quantitative since the average error norm is neither linearly proportional to the identification error nor necessarily a monotonic function of this error. Despite being as arbitrary as, for example, the difference between bifurcation points, this tool is more convenient in practice since it does not require collecting an amount of data for the bifurcation diagram and is especially valuable in case the parameters of the investigated system cannot be changed.

Consider one-directional synchronization of the ODE of the master system

$$\dot{\mathbf{x}}_m = \mathbf{f}(t, \mathbf{x}_m),$$

and the ODE of the slave system:

$$\dot{\mathbf{x}}_{s} = \mathbf{f}(t, \mathbf{x}_{s}) - K(\mathbf{x}_{s} - \mathbf{x}_{m}),$$

where *K* is the matrix of synchronization coefficients.

Once the master system is implemented in analog, a time series could be obtained $\mathbb{X}_m = \{\mathbf{x}_m(t_0), \mathbf{x}_m(t_1), \dots \mathbf{x}_m(t_N)\}$, where N is the overall number of sample points. If the one-step numerical method is used to implement the slave system, a discrete model is obtained:

$$\mathbf{x}_{s,n+1} = \mathbf{x}_{s,n} + \Phi_h(\mathbf{x}_{s,n}, {\mathbf{x}_{m,j}}), j \in [n, n+1].$$

The values $\{\mathbf{x}_{m,j}\}$ refer to the master system states within the time interval $t \in [t_n, t_{n+1}]$, and an index j can be fractional, because one-step method may require auxiliary intermediate sample points, for example, in $t_{n+0.5}$ (as we will see further). The norm of the error between experimental master data series and the slave numerical system is calculated only in the main sample points:

$$\|\Delta \mathbf{x}\|_n = \|\mathbf{x}_{s,n} - \mathbf{x}_{m,n}\|.$$

It was shown in [31] that a generalized synchronization is established between the master and the slave systems, and the mean amplitude of the error norm

$$<\|\Delta\mathbf{x}\|> = \frac{1}{N} \sum_{n=1}^{N} \|\Delta\mathbf{x}\|_n$$

is a measure of how the slave system is close to the master system. A useful metric is also a relative mean synchronization error, defined as

$$e_r = \frac{<\|\Delta\mathbf{x}\|>}{\max\limits_{n\in[1,N]}\|\mathbf{x}_{m,n}\|}.$$

Let the slave system be implemented using the classical Runge–Kutta 4 method (further, an abbreviation RK4 is used). The difference scheme for obtaining the next value $\mathbf{x}_{s,n+1}$ from $\mathbf{x}_{s,n}$ is:

$$\mathbf{k}_{1} = \mathbf{f}(t_{n}, \mathbf{x}_{s,n}) - K(\mathbf{x}_{s,n} - \mathbf{x}_{m}(t_{n})),$$

$$\mathbf{u}_{1} = \mathbf{x}_{s,n} + 0.5h\mathbf{k}_{1},$$

$$\mathbf{k}_{2} = \mathbf{f}(t_{n} + 0.5h, \mathbf{u}_{1} - K(\mathbf{u}_{1} - \mathbf{x}_{m}(t_{n} + 0.5h)),$$

$$\mathbf{u}_{2} = \mathbf{x}_{s,n} + 0.5h\mathbf{k}_{2},$$

$$\mathbf{k}_{3} = \mathbf{f}(t_{n} + 0.5h, \mathbf{u}_{2} - K(\mathbf{u}_{2} - \mathbf{x}_{m}(t_{n} + 0.5h)),$$

$$\mathbf{u}_{3} = \mathbf{x}_{s,n} + h\mathbf{k}_{3},$$

$$\mathbf{k}_{4} = \mathbf{f}(t_{n} + h, \mathbf{u}_{3} - K(\mathbf{u}_{3} - \mathbf{x}_{m}(t_{i+1})),$$

$$\mathbf{x}_{s,n+1} = \mathbf{x}_{s,n} + \frac{h}{6}(\mathbf{k}_{1} + 2\mathbf{k}_{2} + 2\mathbf{k}_{3} + \mathbf{k}_{4}),$$



where $h = t_{n+1} - t_n$ is the time step. The values $\mathbf{x}_m(t_n + 0.5h)$ are unknown from the time series \mathbb{X}_m . One possible way to find them is to downsample the time series by a factor of 2, which is appropriate in case the discretization time step is small enough. Notice that this increases the truncation error of the method $2^4 = 16$ times. Another solution is using multistep methods for obtaining $\mathbf{x}_{s,n+1}$, which is not always convenient for stability reasons. The proposed solution is using four-point Lagrange polynomial:

$$\mathbf{x}_m(t_n + 0.5h) \approx L(t_n + 0.5h),\tag{9}$$

where

$$L(t) = \sum_{j=n-2}^{n+1} \mathbf{x}_{m,j} \prod_{k=n-2, k \neq j}^{n+1} \frac{t - t_k}{t_j - t_k}.$$

To estimate error of this approximation, rewrite (9) as

$$\mathbf{x}_{m}(t_{n}+0.5h) = L(t_{n}+0.5h) + \mathcal{R}(t),$$

where the remainder $\mathcal{R}(t) = \mathcal{O}\left((t_{n+1} - t_{n-2})^4\right)$ provides fourth order of accuracy of estimating $\mathbf{x}_m(t_n + 0.5h)$. If another order of accuracy p is needed, for example, when one uses another Runge–Kutta method of order p, the p-point Lagrange polynomial should be used.

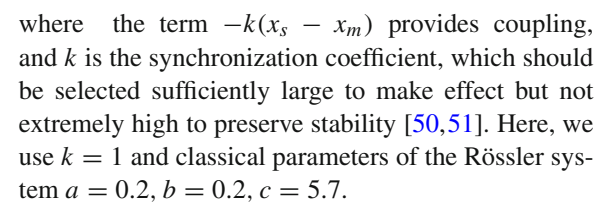
Thus obtained scheme takes advantage of both onestep and multistep approaches: high stability and no need for downsampling. Its disadvantage is that the synchronization error between two discrete models has fourth order of accuracy, while the conventional approach makes it tend to zero. This disadvantage is negligible in the case of synchronization between the real circuit and its model.

As an example, consider the synchronization of two Rössler systems implemented as computer digital models. The master system is described with the following differential equations:

$$\begin{cases} \dot{x}_m &= -y_m - z_m, \\ \dot{y}_m &= x_m + ay_m, \\ \dot{z}_m &= b + z_m (x_m - c), \end{cases}$$
(10)

where x, y, z are state variables and a, b, c are parameters, and the slave system is described by:

$$\begin{cases} \dot{x}_{s} = -y_{s} - z_{s} - k(x_{s} - x_{m}), \\ \dot{y}_{s} = x_{s} + ay_{s}, \\ \dot{z}_{s} = b + z_{s}(x_{s} - c), \end{cases}$$
(11)



Having implemented both systems with RK4 method with a constant stepsize $h = 10^{-5}$ and using Lagrange polynomial for estimating points $\mathbf{x}_m(t_n + 0.5h)$ in the slave system, we obtain the results shown in Fig. 1.

The synchronization error rapidly reaches its steady state with a median value 2.77×10^{-5} . This is relatively high in comparison with ideal synchronization between models when $\mathbf{x}_m(t_i+0.5h)$ are calculated in one solver, allowing obtaining values close to machine epsilon, but pretty enough for our further experiments, which corresponds to a relative error value about $10^{-4}\%$.

2.3 Circuit implementation of the Rössler system

The Rössler system is described by equation (10). In order to implement it as an analog circuit, we first define the simulation time constant $\tau = R_0 C_0$, where R_0 and C_0 refer to parameters of elements in op-amp-based integrators. We select $R_0 = 10 \text{ k}\Omega$ and $C_0 = 10 \text{ nF}$, so $\tau = 10^{-4} \text{ s}$.

Then, we select a scaling factor M, taking into account that real voltage amplitudes should not go out of the range from -10 V to +10 V. We chose the value M=4, making real amplitudes of phase variables implemented as voltages four times smaller than in the original attractor.

Using basic principles of circuit design, we designed the circuit shown in Fig. 2.

The equations of this circuit are as follows:

$$\begin{cases}
C_1 \dot{x} = -\frac{y}{R_1} - \frac{z}{R_2}, \\
C_2 \dot{y} = \frac{x}{R_3} + \frac{y}{R_4}, \\
C_3 \dot{z} = \frac{R_8 V_b}{R_{13}} + \frac{z}{10 R_{13}} \left(\frac{R_{12} x}{R_{10}} - \frac{R_{12} V_c}{R_{11}} \right),
\end{cases} (12)$$

where $R_1 = R_2 = R_3 = R_{11} = R_{12} = R_0$, $R_4 = R_0/a$, $R_5 = R_6$ (arbitrary values close to R_0), $R_8 = MR_0$, $R_{13} = R_0/10$, $R_{10} = R_0/M$, $C_1 = C_2 = C_3 = C_0$. For the Rössler system parameters a = 0.2, b = 0.2 and c = 5.7 and a scaling factor M = 4, we obtain circuit elements listed in Table 1, see the column "Proposed value."

The circuit includes an only configuration with inverting operational amplifiers. The amplifier U_1



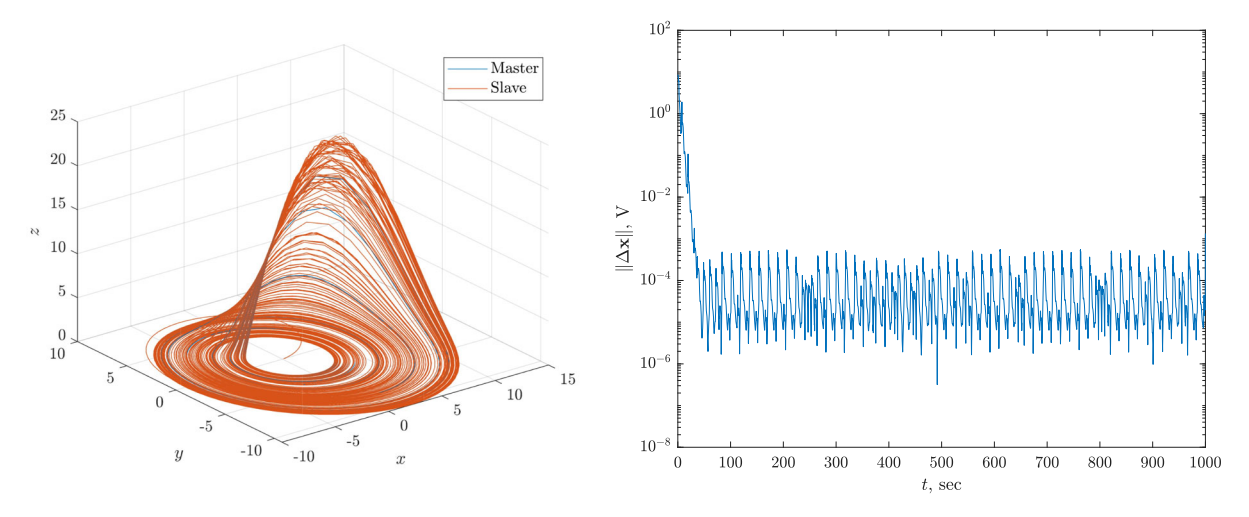


Fig. 1 Numerical example of two Rössler systems synchronization. Both systems are implemented using the RK4 method. The master system intermediate points $\mathbf{x}_m(t_n+0.5h)$ used for estimating the slave system states are found from data using the Lagrange interpolation polynomials. Left panel shows the system attractor,

both trajectories visually coincide almost everywhere. The right panel shows the synchronization error: It rapidly decays during the initial transient process and then oscillates near a median value 2.77×10^{-5}

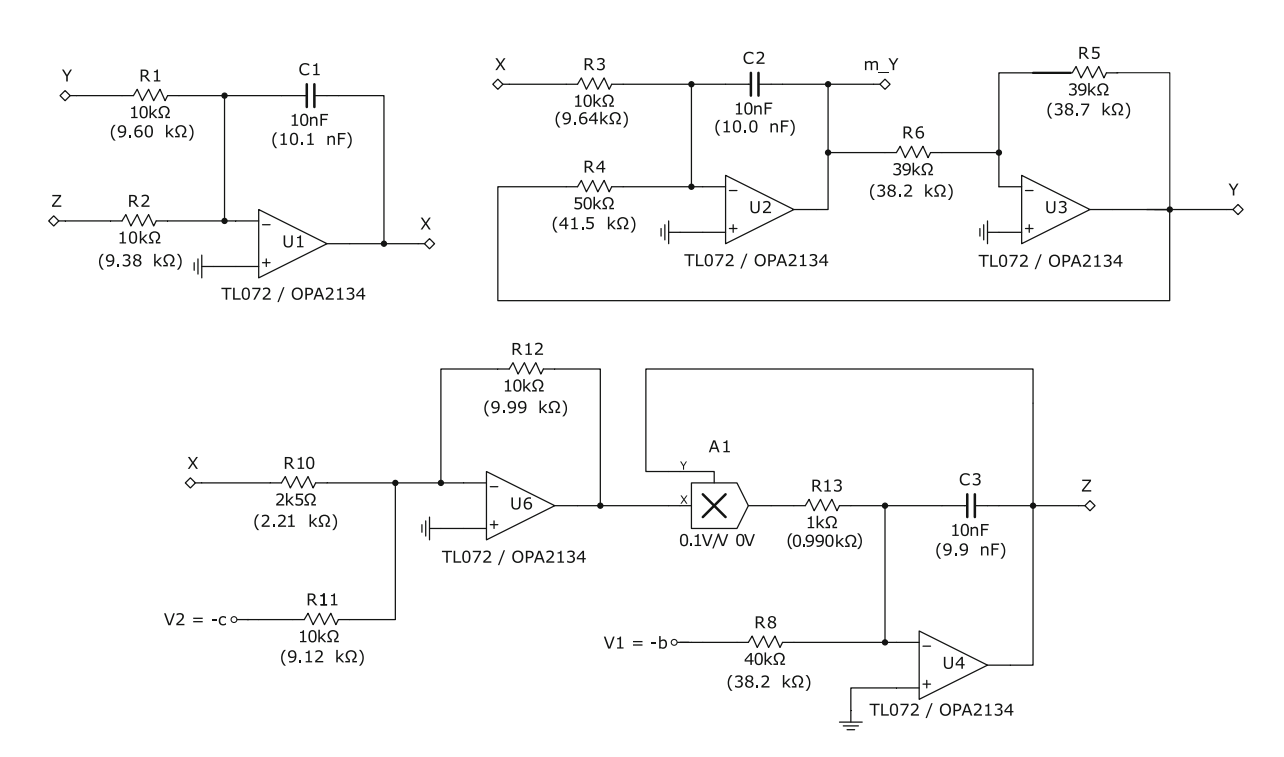


Fig. 2 Rössler system circuit implementation. Real measured values of components are given in brackets. Power supply voltages are $V_{CC-} = -10$ V and $V_{CC+} = +10$ V. Additional offset

voltages V1 = -0.2 V and V1 = -5.7V are used for introducing parameters b and c



Table 1 Proposed and real measured values of the circuit elements used in the experiment

R1 10 9.60 ± 0.12 R2 10 9.38 ± 0.12 R3 10 9.64 ± 0.12 R4 40 41.5 ± 0.5 R5 39 38.7 ± 0.5 R6 39 38.2 ± 0.5 R8 40 38.2 ± 0.5 R10 2.5 2.21 ± 0.03 R11 10 9.12 ± 0.12 R12 10 9.99 ± 0.12 R13 1 0.990 ± 0.013	Units	Error	Measured value	Proposed value	Element
R3 10 9.64 ± 0.12 R4 40 41.5 ± 0.5 R5 39 38.7 ± 0.5 R6 39 38.2 ± 0.5 R8 40 38.2 ± 0.5 R10 2.5 2.21 ± 0.03 R11 10 9.12 ± 0.12 R12 10 9.99 ± 0.12	kΩ	± 0.12	9.60	10	R1
R4 40 41.5 ± 0.5 R5 39 38.7 ± 0.5 R6 39 38.2 ± 0.5 R8 40 38.2 ± 0.5 R10 2.5 2.21 ± 0.03 R11 10 9.12 ± 0.12 R12 10 9.99 ± 0.12	$k\Omega$	± 0.12	9.38	10	R2
R5 39 38.7 ± 0.5 R6 39 38.2 ± 0.5 R8 40 38.2 ± 0.5 R10 2.5 2.21 ± 0.03 R11 10 9.12 ± 0.12 R12 10 9.99 ± 0.12	$k\Omega$	± 0.12	9.64	10	R3
R6 39 38.2 \pm 0.5 R8 40 38.2 \pm 0.5 R10 2.5 2.21 \pm 0.03 R11 10 9.12 \pm 0.12 R12 10 9.99 \pm 0.12	$k\Omega$	± 0.5	41.5	40	R4
R8 40 38.2 \pm 0.5 R10 2.5 2.21 \pm 0.03 R11 10 9.12 \pm 0.12 R12 10 9.99 \pm 0.12	$k\Omega$	± 0.5	38.7	39	R5
R10 2.5 2.21 \pm 0.03 R11 10 9.12 \pm 0.12 R12 10 9.99 \pm 0.12	$k\Omega$	± 0.5	38.2	39	R6
R11 10 9.12 \pm 0.12 R12 10 9.99 \pm 0.12	$k\Omega$	± 0.5	38.2	40	R8
R12 10 9.99 ± 0.12	$k\Omega$	± 0.03	2.21	2.5	R10
	$k\Omega$	± 0.12	9.12	10	R11
R13 1 0.990 \pm 0.013	$k\Omega$	± 0.12	9.99	10	R12
	$k\Omega$	± 0.013	0.990	1	R13
C1 10 10.1 ± 0.3	nF	± 0.3	10.1	10	C1
C2 10 10.0 ± 0.3	nF	± 0.3	10.0	10	C2
C3 10 9.9 ± 0.3	nF	± 0.3	9.9	10	C3

refers to the first line of Eq. (12), the amplifiers U_2 and U_3 refer to the second line of (12): U_2 is used for summation and integration, and U_3 inverses the sign of y. The amplifier U_6 performs summation and U_4 sums and integrates, implementing the third line of (12).

Two variants of low-distortion low-noise op-amp ICs are used: OPA2134 and TL072 (both manufactured by Texas Instruments).

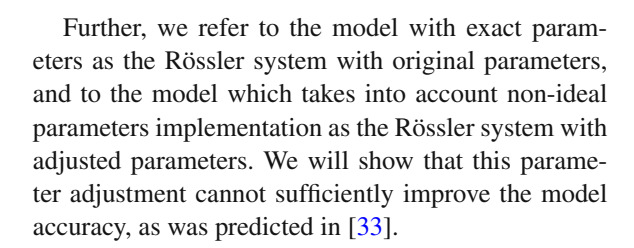
The multiplier AD633 has five signal inputs X_1 , X_2 , Y_1 , Y_2 , Z, allowing performing the following operation:

$$W = (X_1 - X_2)(Y_1 - Y_2)/10 + Z.$$
(13)

It can be used for performing one addition, two subtractions, and one multiplication. Nevertheless, in order to exclude any effect of its internal structure on summation and subtractions, we use it only for multiplication, and addition is performed on an operational amplifier.

Parameters $V_1 = b$ and $V_2 = c$ are set as DAC outputs of the NI ELVIS III laboratory station.

Practical implementation of the circuit with non-ideal components leads to a mismatch between proposed and real values of circuit elements. Table 1 figures our real parameters of the resistors and capacitors, measured with RLC-meter DT-9930, see the column "Real value." The instrumental error of the RLC-meter is ± 1.2 and $\pm 3.0\%$ for resistance and capacitance measurements, respectively.

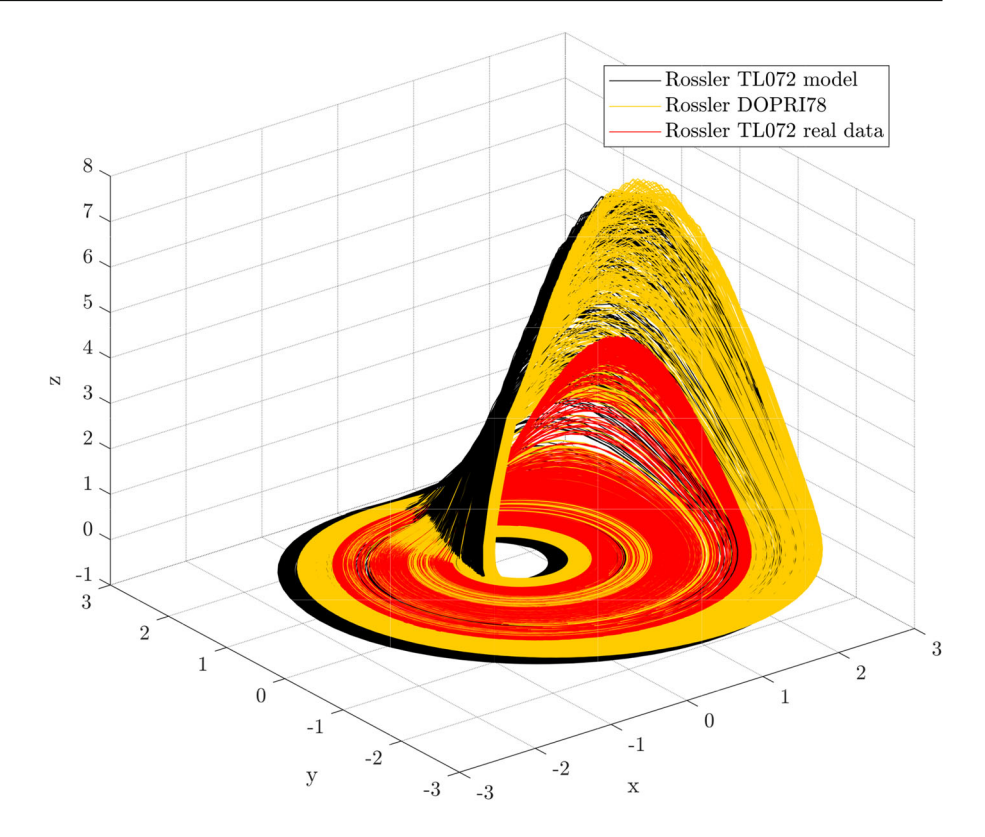


3 Experimental results

This section describes the experimental results of the study. First, we investigate geometric parameters of the chaotic attractors for the real circuit, conventional ODE system and a SPICE model developed in Multisim 14.2 software environment by National Instruments. Further, the latter model will be called the Multisim model for brevity. Solving ODE is carried out using the Dormand-Prince 8(7) method, further referred to as DOPRI78 after a well-known program [52]. Then, we estimate the error the model obtained via the proposed technique and compare it with the errors of the conventional ODE and NI Multisim model. The experiments confirm that the proposed technique provides the most relevant model among the considered ones. Finally, we present obtained models of two variants of the circuit each containing 60 independent terms and coefficients.



Fig. 3 Attractor of the Rössler circuit in NI Multisim simulation environment, solution of the circuit ODE with adjusted parameters and attractor of the real circuit with TL072 op-amp and AD633JN analog multiplier



3.1 Geometry of real and simulated attractors

Due to the imperfectness of real resistors and capacitors, their values would necessarily possess a deviation of the obtained attractor from the trajectories of the original one as shown in Fig. 1a. Therefore, we will use models with adjusted parameters in further experiments.

All real-time series have length 0.1 sec. It is equivalent to 1000 s of the original Rössler system (10) up to a simulation time constant $\tau = R_0C_0 = 10^{-4}$ sec, defined in Sect. 2.3. Amplitude values are decreased by a scaling factor M = 4 compared to the original system (10) for reasons of feasibility, as was also defined in Sect. 2.3.

The first comparison involves the solution of the Eq. (12) with the DOPRI78 method using fixed stepsize $h = 10^{-5}$, the model of the circuit shown in Fig. 2 in NI Multisim 14.2 circuit simulation environment, and the real circuit built on NI ELVIS III prototyping board. Operational amplifiers TL072 were used. The corresponding three attractors are shown in Fig. 3. The trajectory given in yellow is obtained via solving the Rössler ODE with adjusted parameters. The trajectory given in black is obtained in NI Multisim 14.2 environment. One can see that these trajectories are close to each other which confirms that these models are in good correspondence. Nevertheless, the trajectory obtained from the circuit given in red is sufficiently different. While keeping an almost similar shape, it has lower amplitudes in all variables.

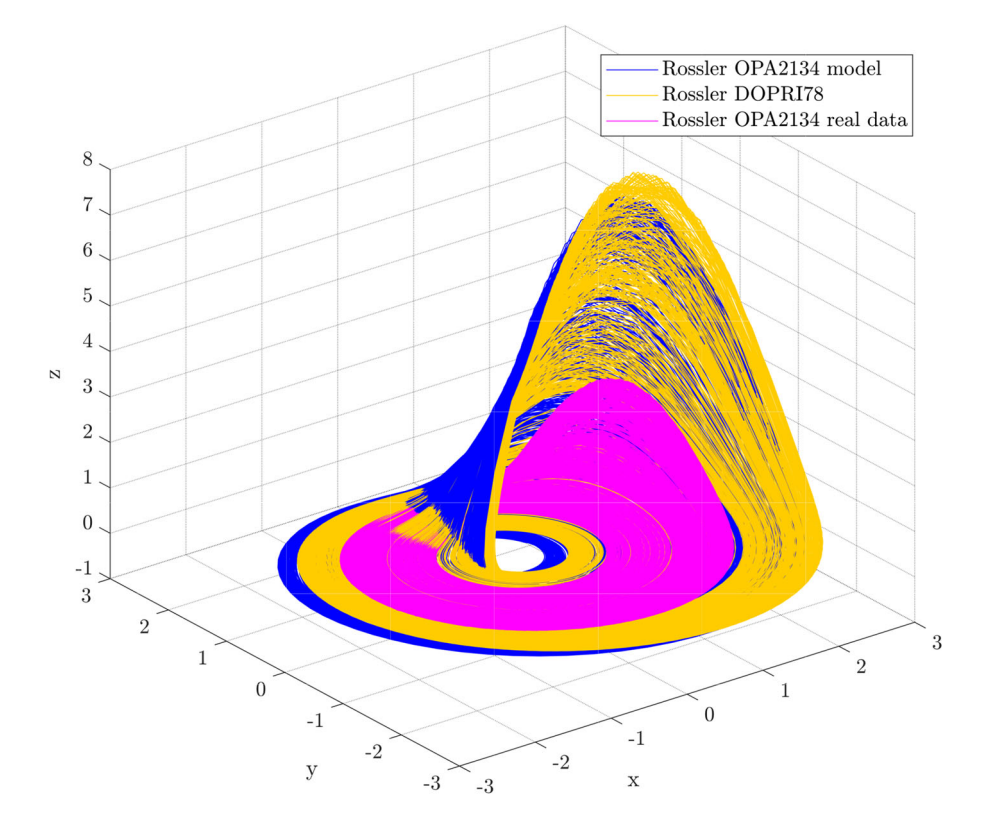
The obtained results provide evidence that the real analog system sufficiently differs from the ODE it was intended to simulate. Besides, the internal structure of active component models used in NI Multisim is fairly simple, giving only a slight difference from ODE in the resulting trajectory.

Cognate conclusions can be drawn from the comparison of the circuit with OPA2134 operational amplifiers and two other models; see Fig. 4. The trajectory of Eq. (12) solved with the DOPRI78 method is given in blue, the trajectory of the NI Multisim model is given in yellow, and the data from the circuit are plotted violet.

To provide a representative comparison of attractor geometry, we estimated the amplitudes of each state variable Δx , Δy , Δz and calculated volumes of circumscribed parallelepipeds for the attractors $V = \Delta x \Delta y \Delta z$. The following models were stud-



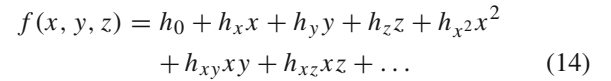
Fig. 4 Attractor of Rössler ODE with adjusted parameters, Multisim simulation and real circuit, OPA2134 op-amp and AD633JN analog multiplier are used



ied: the adjusted Rössler model, the Multisim simulation with TL072 op-amp, the Multisim simulation with OPA2134 op-amp, the circuit with TL072 op-amp, and the circuit with OPA2134 op-amp. These values are given in Table 2. The difference in the variable z is the most significant. The attractor volumes of real circuits and models differ more than two times.

3.2 Model error estimation

Using the system identification technique outlined in Sect. 2.1, we obtained the models for the following systems: the Rössler circuit ODE with original parameters, the Rössler circuit ODE with adjusted parameters, the Multisim model with TL072 op-amp, the Multisim model with OPA2134 op-amp, the real circuit with TL072 op-amp, the real circuit with OPA2134 op-amp. For brevity, we do not present the models except the two most important ones: the models of the real circuits with TL072 and OPA2134 op-amps. Coefficients of right-hand side functions of the corresponding system of ODEs are given in Table 3 in the following form:



The monomials in f(x, y, z) are given in degree-lexicographic order. With the powers of monomials from 0 to 3, the function (14) contains 20 terms. The parameters of the Algorithm 1 were $\eta=10^{-5}$ and $\varepsilon=10^{-5}$.

The synchronization-based approach described in Sect. 2.2 was applied to estimate the accuracy of the obtained models. For verifying that the obtained models are indeed more relevant than the Rössler ODEs (original and with adjusted parameters), they were also used in synchronization-based accuracy tests.

The results are summarized in two tables. Table 4 gives the results of 12 experiments carried out to estimate the relevancy of the Rössler ODE to the real circuit and its model. Median and mean absolute synchronization errors are given, as well as a mean relative synchronization error in percent. The lowest obtained errors correspond to synchronization errors between similar models in the form of ODE, as expected. The order of relative error about $10^{-4}\%$ is a theoretical minimum for the RK4 method with Lagrange interpolation of the



Table 2 Attractor geometric parameters: Δx , Δy , Δz are difference between maximal and minimal values obtained in the experiment, V is a volume of a circumscribed parallelepiped $V = \Delta x \Delta y \Delta z$

System	Δx	Δy	Δz	V
Rössler ODE (real components)	5.18 ± 0.03	4.74 ± 0.03	7.66 ± 0.18	188 ± 6
Multisim, TL072	5.18 ± 0.02	4.79 ± 0.04	7.61 ± 0.14	189 ± 5
Multisim, OPA2134	5.15 ± 0.03	4.75 ± 0.03	7.31 ± 0.15	179 ± 6
Circuit, TL072	4.26 ± 0.01	3.93 ± 0.01	3.92 ± 0.04	65.8 ± 0.6
Circuit, OPA2134	3.98 ± 0.01	3.70 ± 0.01	2.89 ± 0.05	42.4 ± 0.9

All confidence intervals are 95%

Table 3 Coefficients of the models obtained from the circuits with TL072 and OPA2134 operational amplifiers

Coefficient	TL072			OPA2134		
	\dot{x}	ý	ż	\dot{x}	ý	ż
h_0	1.9849 ×10 ⁻²	-2.4084×10^{-3}	6.2474 ×10 ⁻²	2.3157×10^{-2}	5.0043 ×10 ⁻²	0.0514
h_X	1.7621×10^{-2}	1.0191	-7.6250×10^{-3}	1.9581×10^{-2}	1.0210	-6.8586×10^{-3}
h_y	-0.99030	0.17204	4.6164×10^{-3}	-0.98931	0.17253	8.5437×10^{-3}
h_z	-1.4570	-6.8364×10^{-2}	-5.6767	-1.4324	-8.0235×10^{-2}	-5.5735
h_{χ^2}	1.0702×10^{-3}	4.4290×10^{-4}	3.6258×10^{-4}	-8.3903×10^{-4}	1.3080×10^{-4}	-2.7385×10^{-3}
h_{xy}	-1.7098×10^{-3}	-4.0747×10^{-4}	-1.8867×10^{-3}	-2.3521×10^{-3}	-2.2361×10^{-4}	-1.2921×10^{-3}
h_{xz}	0.18730	3.9947×10^{-2}	4.2853	0.21910	1.7422×10^{-2}	4.4341
h_{y^2}	-8.3531×10^{-4}	5.3668×10^{-4}	-2.9468×10^{-3}	-1.7882×10^{-3}	6.2991×10^{-4}	-2.9647×10^{-3}
h_{yz}	4.8575×10^{-2}	2.1055×10^{-2}	-0.48176	3.2884×10^{-2}	1.9215×10^{-2}	-0.64099
h_{z^2}	-4.2236×10^{-3}	5.6370×10^{-5}	-0.39533	-2.0921×10^{-2}	1.1762×10^{-2}	-0.47623
h_{x^3}	1.6788×10^{-3}	-4.0500×10^{-3}	2.3340×10^{-4}	1.0614×10^{-3}	-3.5939×10^{-3}	-2.9115×10^{-3}
h_{x^2y}	1.7380×10^{-3}	-4.8882×10^{-3}	-8.0567×10^{-4}	-9.7620×10^{-4}	-4.8569×10^{-3}	-1.0696×10^{-3}
h_{x^2z}	6.9154×10^{-2}	-9.1399×10^{-3}	0.17589	6.1403×10^{-2}	2.9867×10^{-3}	8.9730×10^{-2}
h_{xy^2}	-2.8329×10^{-3}	-3.7991×10^{-3}	-9.3897×10^{-4}	-4.1564×10^{-3}	-2.3594×10^{-3}	-1.5386×10^{-3}
h_{xyz}	2.4123×10^{-2}	-9.8508×10^{-3}	0.13015	1.6979×10^{-2}	-3.8066×10^{-3}	0.13526
h_{xz^2}	-1.3913×10^{-2}	-8.2434×10^{-4}	-7.1060×10^{-3}	-1.4069×10^{-2}	-4.5071×10^{-3}	3.3169×10^{-2}
h_{y^3}	2.6073×10^{-3}	2.5179×10^{-4}	-1.2808×10^{-3}	1.7447×10^{-3}	7.7572×10^{-4}	-1.2008×10^{-3}
h_{y^2z}	8.4769×10^{-3}	-1.0925×10^{-2}	3.6443×10^{-2}	3.1421×10^{-3}	-3.3616×10^{-3}	4.8279×10^{-2}
h_{yz^2}	2.9241×10^{-2}	-3.4983×10^{-3}	9.4090×10^{-2}	3.6882×10^{-2}	-2.2363×10^{-3}	0.10730
h_{z^3}	6.7338×10^{-3}	-4.1591×10^{-5}	2.2279×10^{-2}	1.1082×10^{-2}	-9.0613×10^{-4}	2.5367×10^{-2}

middle point and the stepsize $h=10^{-5}$. The errors between ODEs and other systems are relatively large, about 6–8% for the ODE with original parameters and 3–8% for the ODE with adjusted parameters.

Table 5 summarizes the results of 6 other experiments with synchronization of the data obtained from various systems and the models obtained via the proposed approach. It is of interest that parameters of the identification algorithm $\varepsilon = \eta = 10^{-5}$ lead to a similar error between ODEs and real data from circuits. One

more interesting observation on that Multisim results are not identified well, which originates from simulation errors introduced in this software package by both adaptive stepsize control algorithm and low accuracy of the trapezoidal method used for simulation.

To visualize the results of synchronization experiments, we present the error plots in logarithmic scale in Fig. 5. Panel (a) shows the synchronization error between the circuit with OPA2134 and its model obtained via the proposed technique, panel (b) gives



 Table 4
 Synchronization errors between real data and models based on original Rössler ODE

System	Rössler ODE, original parameters			Rössler ODE, adjusted parameters		
	Median	Mean	Mean, %	Median	Mean	Mean, %
Rössler orig. ODE	2.5626×10^{-5}	6.4179 ×10 ⁻⁵	2.7265 ×10 ⁻⁴	0.25598	0.4448	7.5591
Rössler adjusted ODE	0.9263	1.5463	4.8483	1.0684×10^{-5}	2.6749×10^{-4}	3.3547×10^{-4}
Multisim, TL072	1.6127	1.8167	5.9581	0.4194	0.6190	8.121
Multisim, OPA2134	1.9420	1.6075	6.5933	0.3863	0.3891	5.2847
Circuit, TL072	0.56914	1.0487	6.1491	0.14096	0.11889	3.3063
Circuit, OPA2134	0.88045	1.1895	8.9829	0.18727	0.20016	6.0461

Table 5 Synchronization errors between the data collected from various systems and the models reconstructed with the proposed algorithm

System (data source)	Median	Mean	Mean, %
Rössler orig. ODE	5.1217×10^{-3}	9.4747×10^{-3}	4.0250×10^{-2}
Rössler adjusted ODE	2.6192×10^{-3}	6.6841×10^{-3}	8.3827×10^{-2}
Multisim, TL072	6.9212×10^{-2}	0.1249	1.6389
Multisim, OPA2134	3.0144×10^{-2}	3.3475×10^{-2}	0.4546
Circuit, TL072	9.7622×10^{-3}	1.3091×10^{-2}	7.6764×10^{-2}
Circuit, OPA2134	7.7741×10^{-3}	9.3596×10^{-3}	7.0681×10^{-2}

the synchronization error between the same circuit and ODE with adjusted parameters, the panels (c) and (d) give the comparison of the model obtained by the proposed technique and the conventional ODE for the circuit with TL072. The behavior of the synchronization error trajectory is not uniform, and the more accurate model has larger dispersion but a lower average value.

The attractors of the real circuits and the obtained models are shown in Fig. 6. One can see the visual difference between the attractors of the systems implemented using different operational amplifiers. The identified models replicate the shapes of the original attractors, as can be seen in panels (a) and (c). Adding synchronization allows one to obtain visually coinciding fragments of trajectories, especially near z=0 plane where the local divergence of trajectories is the lowest.

4 Discussion and conclusions

Chaotic systems can be implemented in various ways, one of which is a chaotic analog circuit. However, it is known that real circuit behavior always deviates from the simulated one. The discrepancy between the chaotic

circuit and its model has been reported many times in the literature, just a few examples can be found in [31,33,34]. This discrepancy results in difficulties with the design and operation of the chaotic circuits, as well as in limiting the validity of transition from the ODE to the circuit. To address the problem, we propose finding an empirical ODE of the circuit using a special system identification technique. Thus, obtained ODE represents a white-box model, from which coefficient distortion and additional nonlinearities emerging in the circuit can be explicitly found, and the accuracy of the desired system implementation can be estimated. In practical applications, this ODE may be used instead of the original ODE and the SPICE model.

As an experimental result of the study, we present 60-term models of two Rössler chaotic circuit implementations with TL072 and OPA2134 operational amplifiers, respectively, which give notably different attractors for similar parameters in the original ODE. An elaborate study was carried out to verify that these models are the most accurate models among all investigated ones including also conventional ODEs and SPICE models in NI Multisim 14.2 software environment.



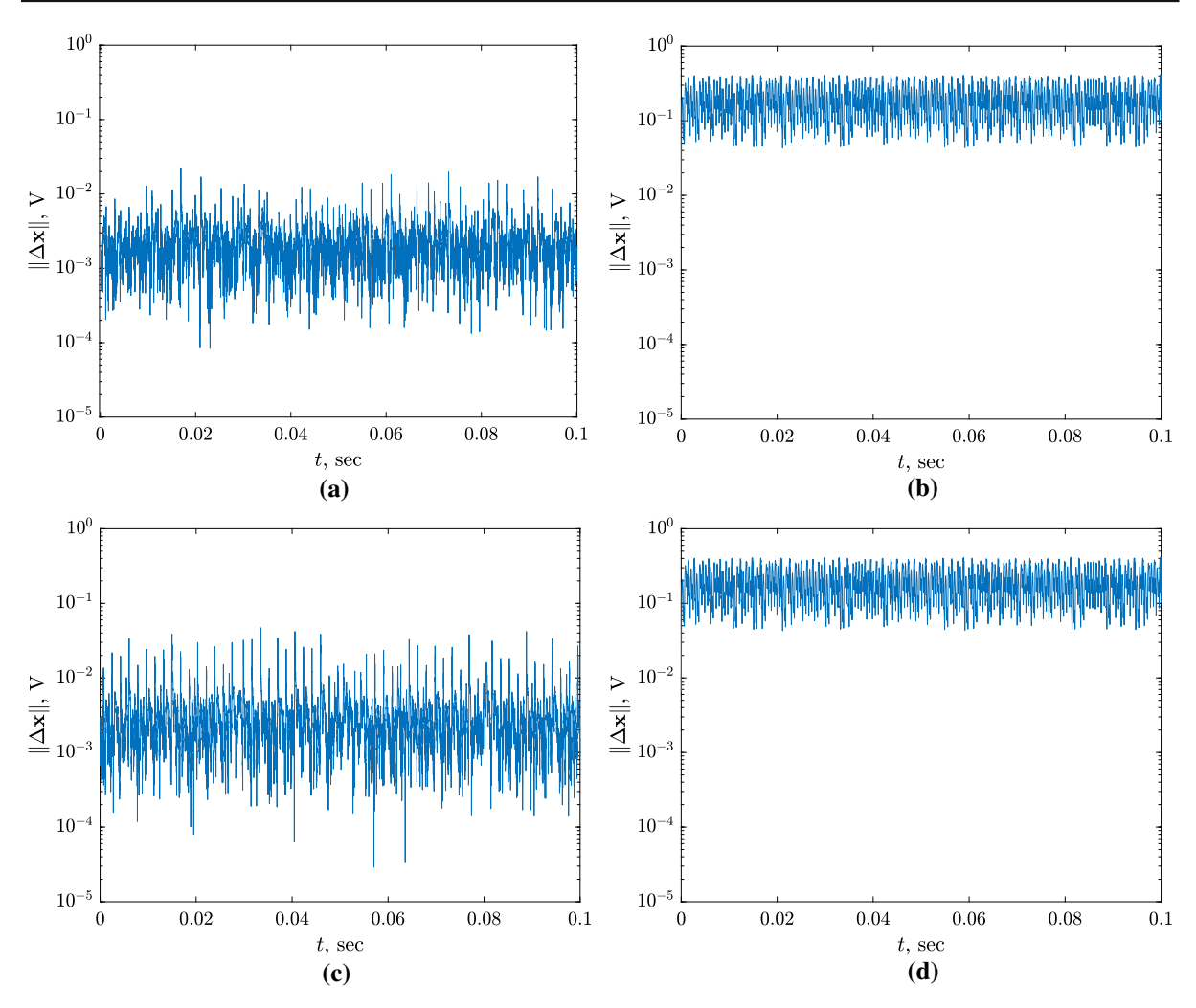


Fig. 5 Synchronization errors of **a** the Rössler circuit with OPA2134 and its model obtained via the proposed technique, **b** Rössler circuit with OPA2134 and its model in the form of the adjusted Rössler ODE, **c** the Rössler circuit with TL072 and

its model obtained via the proposed technique, **d** Rössler circuit with TL072 and its model in the form of the adjusted Rössler ODE. All figures are of the same scale

The theoretical contribution of our work is in establishing a way to simulate real circuit behavior more accurately in terms of keeping the model trajectories in the vicinity of the experimental trajectories. The importance of studying more accurate models is undoubted in chaotic systems. While in the investigated case of the Rössler system the difference between the conventional computer models and the circuit was only quantitative, the nature of chaos prompts us that there could be a more notable disparity in other cases. For example, coexisting and hidden attractors observed in analytical ODE could not be observed in a circuit, or chaotic

behavior in an ODE could correspond to non-chaotic behavior in the circuit for the same set of parameters.

The practical relevance of the reported study is that the accurate models obtained via the proposed technique can be used to generate a signal similar to the output of a real circuit, which results in accurate analog-to-digital synchronization that was explicitly shown in this study. Accurate analog-to-digital synchronization can be used in many possible applications, where the fundamental property of chaotic synchronization is utilized. Examples of such applications are chaotic sensing and chaotic communication systems. The reported



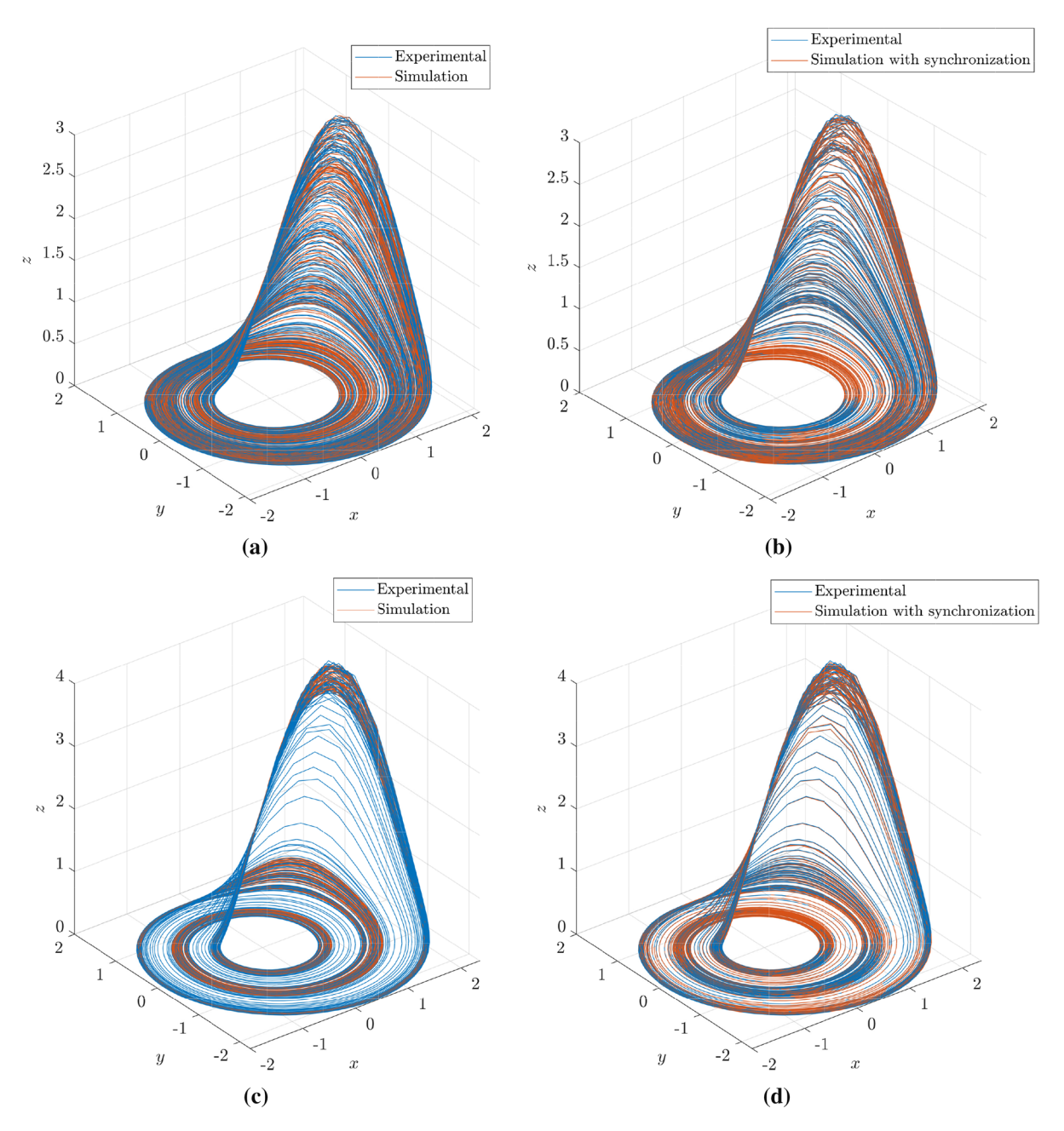


Fig. 6 Attractors of **a** the Rössler circuit with OPA2134 (Experimental) and its identified model (Simulation), **b** the Rössler circuit with OPA2134 (Experimental) and its model synchronized with real data (Simulation with synchronization), **c** the Rössler

circuit with TL072 (Experimental) and its model (Simulation), d the Rössler circuit with TL072 (Experimental) and its model synchronized with real data (Simulation with synchronization)

identification algorithm can also be used for time series reconstruction and a cryptographic attack on chaosbased encryption systems. Another interesting branch of research is connected with studies on how the proposed models can reproduce the sensitivity of the circuit to noise inherent to real circuits, which can sufficiently affect the system behavior, as shown in several recent works, e.g., [24,53,54]. Our future work will



be dedicated to some of these phenomena and applica-

Funding This study was supported by the grant of the Russian Science Foundation (RSF), Project 22-19-00573.

Availability of data and materials The data collected in this study are available from the corresponding author on reasonable request.

Declarations

Conflict of interest The authors declare that they have no conflict of interest.

References

- Meyers, R.A.: Encyclopedia of Physical Science and Technology. Academic Press (2002)
- Karimov, T., Nepomuceno, E.G., Druzhina, O., Karimov, A., Butusov, D.: Chaotic oscillators as inductive sensors: theory and practice. Sensors 19(19), 4314 (2019)
- 3. Chua, L., Komuro, M., Matsumoto, T.: The double scroll family. IEEE Trans. Circuits Syst. 33(11), 1072 (1986)
- Kennedy, M.P.: Three steps to chaos. II. A Chua's circuit primer. IEEE Trans. Circuits Syst. I: Fundam. Theory Appl. 40(10), 657 (1993)
- Kennedy, M., Chua, L.: Van der Pol and chaos. IEEE Trans. Circuits Syst. 33(10), 974 (1986)
- Lai, Q., Wan, Z., Kuate, P.D.K., Fotsin, H.: Coexisting attractors, circuit implementation and synchronization control of a new chaotic system evolved from the simplest memristor chaotic circuit. Commun. Nonlinear Sci. Numer. Simul. 89, 105341 (2020)
- Wang, M., Liao, X., Deng, Y., Li, Z., Su, Y., Zeng, Y.: Dynamics, synchronization and circuit implementation of a simple fractional-order chaotic system with hidden attractors. Chaos, Solitons Fractals 130, 109406 (2020)
- 8. Wang, X., Pham, V.T., Jafari, S., Volos, C., Munoz-Pacheco, J.M., Tlelo-Cuautle, E.: A new chaotic system with stable equilibrium: from theoretical model to circuit implementation. IEEE Access 5, 8851 (2017)
- Sambas, A., Vaidyanathan, S., Zhang, S., Zeng, Y., Mohamed, M.A., Mamat, M.: A new double-wing chaotic system with coexisting attractors and line equilibrium: bifurcation analysis and electronic circuit simulation. IEEE Access 7, 115454 (2019)
- Rahman, Z.A.S., Jasim, B.H., Al-Yasir, Y.I., Hu, Y.F., Abd-Alhameed, R.A., Alhasnawi, B.N.: A new fractional-order chaotic system with its analysis, synchronization, and circuit realization for secure communication applications. Mathematics 9(20), 2593 (2021)
- Chen, S.B., Jahanshahi, H., Abba, O.A., Solís-Pérez, J., Bekiros, S., Gómez-Aguilar, J., Yousefpour, A., Chu, Y.M.: The effect of market confidence on a financial system from the perspective of fractional calculus: Numerical investigation and circuit realization. Chaos, Solitons Fractals 140, 110223 (2020)

- Lassoued, A., Boubaker, O., Dhifaoui, R., Jafari, S.: Experimental observations and circuit realization of a jerk chaotic system with piecewise nonlinear function. In: Recent Advances in Chaotic Systems and Synchronization, pp. 3–21. Elsevier (2019)
- 13. Lai, Q., Bao, B., Chen, C., Kengne, J., Akgul, A.: Circuit application of chaotic systems: modeling, dynamical analysis and control. In: The European Physical Journal Special Topics. Springer (2021)
- Petrzela, J., Polak, L.: Minimal realizations of autonomous chaotic oscillators based on trans-immittance filters. IEEE Access 7, 17561 (2019)
- Minati, L., Frasca, M., Oświecimka, P., Faes, L., Drożdż, S.: Atypical transistor-based chaotic oscillators: design, realization, and diversity. Chaos: Interdiscipl. J. Nonlinear Sci. 27(7), 073113 (2017)
- Wu, R., Wang, C.: A new simple chaotic circuit based on memristor. Int. J. Bifurc. Chaos 26(09), 1650145 (2016)
- Sprott, J.C.: Simple chaotic systems and circuits. Am. J. Phys. 68(8), 758 (2000)
- Dalkiran, F.Y., Sprott, J.C.: Simple chaotic hyperjerk system. Int. J. Bifurc. Chaos 26(11), 1650189 (2016)
- Yao, J., Wang, K., Huang, P., Chen, L., Machado, J.T.: Analysis and implementation of fractional-order chaotic system with standard components. J. Adv. Res. 25, 97 (2020)
- 20. Sprott, J.C.: A new chaotic jerk circuit. IEEE Trans. Circuits Syst. II Express Br. **58**(4), 240 (2011)
- Wang, Y., Min, F., Cheng, Y., Dou, Y.: Dynamical analysis in dual-memristor-based FitzHugh–Nagumo circuit and its coupling finite-time synchronization. Eur. Phys. J. Spec. Top. 230(7), 1751 (2021)
- Fan, T., Tuo, X., Li, H., He, P.: Chaos control and circuit implementation of a class of double-wing chaotic system. Int. J. Numer. Model. Electron. Netw. Devices Fields 32(5), 240 (2019)
- Wang, G., Chen, D., Lin, J., Chen, X.: The application of chaotic oscillators to weak signal detection. IEEE Trans. Industr. Electron. 46(2), 440 (1999)
- Silva, I.G., Korneta, W., Stavrinides, S.G., Picos, R., Chua, L.O.: Observation of stochastic resonance for weak periodic magnetic field signal using a chaotic system. Commun. Nonlinear Sci. Numer. Simul. 94, 105558 (2021)
- Karimov, T., Druzhina, O., Karimov, A., Tutueva, A., Ostrovskii, V., Rybin, V., Butusov, D.: Single-coil metal detector based on spiking chaotic oscillator. Nonlinear Dyn. 107(1), 1295 (2022)
- Xiong, L., Lu, Y.J., Zhang, Y.F., Zhang, X.G., Gupta,
 P.: Design and hardware implementation of a new chaotic secure communication technique. PLoS One 11(8), e0158348 (2016)
- Kocamaz, U.E., Çiçek, S., Uyaroğlu, Y.: Secure communication with chaos and electronic circuit design using passivity-based synchronization. J. Circuits, Syst. Comput. 27(04), 1850057 (2018)
- Williams, I.: "Trust, but verify" SPICE model accuracy, part 1: common-mode rejection ratio. https://e2e.ti.com/blogs_/b/analogwire/posts/trust-but-verify-spice-mod del-daccuracy-part-1-common-mode-rejection-ratio-cmrr (2017). Accessed 18 Apr 2022



 Nazaré, T.E., Nepomuceno, E.G., Martins, S.A., Butusov, D.N.: A note on the reproducibility of chaos simulation. Entropy 22(9), 953 (2020)

- Kiers, K., Schmidt, D., Sprott, J.C.: Precision measurements of a simple chaotic circuit. Am. J. Phys. 72(4), 503 (2004)
- Karimov, A., Tutueva, A., Karimov, T., Druzhina, O., Butusov, D.: Adaptive generalized synchronization between circuit and computer implementations of the Rössler system. Appl. Sci. 11(1), 81 (2020)
- Karimov, T.I., Druzhina, O.S., Karimov, A.I., Kolev, G.Y., Butusov, D.N.: Comparison of bifurcation diagrams for numerical and analog chaotic systems. In: 2021 IEEE Conference of Russian Young Researchers in Electrical and Electronic Engineering (ElConRus). IEEE, pp. 124–128 (2021)
- Karimov, T., Butusov, D., Andreev, V., Karimov, A., Tutueva, A.: Accurate synchronization of digital and analog chaotic systems by parameters re-identification. Electronics 7(7), 123 (2018)
- Butusov, D.N., Karimov, T.I., Lizunova, I.A., Soldatkina, A.A., Popova, E.N.: Synchronization of analog and discrete Rössler chaotic systems. In: 2017 IEEE Conference of Russian Young Researchers in Electrical and Electronic Engineering (EIConRus). IEEE, pp. 265–270 (2017)
- Kera, H., Hasegawa, Y.: Noise-tolerant algebraic method for reconstruction of nonlinear dynamical systems. Nonlinear Dyn. 85(1), 675 (2016)
- Karimov, A., Nepomuceno, E.G., Tutueva, A., Butusov,
 D.: Algebraic method for the reconstruction of partially observed nonlinear systems using differential and integral embedding. Mathematics 8(2), 300 (2020)
- Brunton, S.L., Proctor, J.L., Kutz, J.N.: Discovering governing equations from data by sparse identification of nonlinear dynamical systems. Proc. Natl. Acad. Sci. 113(15), 3932 (2016)
- Karimov, A.I., Kopets, E., Nepomuceno, E.G., Butusov,
 D.: Integrate-and-differentiate approach to nonlinear system identification. Mathematics 9(23), 2999 (2021)
- Eichas, F.: System identification of nonlinear audio circuits.
 Ph.D. thesis, Allgemeine Nachrichtentechnik (2020)
- Fukami, K., Murata, T., Zhang, K., Fukagata, K.: Sparse identification of nonlinear dynamics with lowdimensionalized flow representations. J. Fluid Mech. 926 (2021)
- Ibrahim, K., Jamal, R., Ali, F.: Chaotic behaviour of the Rossler model and its analysis by using bifurcations of limit cycles and chaotic attractors. J. Phys: Confer. Ser. 1003(1), 012099 (2018)
- Jaimes-Reategui, R., Sevilla-Escoboza, R., Pisarchik, A., Garcia, J., Huerta-Cuellar, G., Ruiz-Oliveras, F., Lopez-Mancilla, D., Castaneda, C.: Secure optoelectronic communication using laser diode driving by chaotic Rössler oscillators. J. Phys: Confer. Ser. 274, 012024 (2011). https://doi.org/10.1088/1742-6596/274/1/012024
- Larptwee, S., San-Um, W.: Implementation of Rössler chaotic system through inherent exponential nonlinearity of a diode with two-channel chaotic synchronization applications. In: 2013 4th International Conference on Intelligent Control and Information Processing (ICICIP). IEEE, pp. 787–791 (2013)

- 44. Limbeck, J.: Computation of approximate border bases and applications. Ph.D. thesis, Universität Passau (2013)
- Livni, R., Lehavi, D., Schein, S., Nachliely, H., Shalev-Shwartz, S., Globerson, A.: Vanishing component analysis.
 In: International Conference on Machine Learning. PMLR, pp. 597–605 (2013)
- Yan, H., Yan, Z., Xiao, G., Wang, W., Zuo, W.: Deep vanishing component analysis network for pattern classification. Neurocomputing 316, 240 (2018)
- Cox, D., Little, J., OShea, D.: Ideals, Varieties, and Algorithms: An Introduction to Computational Algebraic Geometry and Commutative Algebra. Springer (2013)
- Cortiella, A., Park, K.C., Doostan, A.: Sparse identification of nonlinear dynamical systems via reweighted ℓ1-regularized least squares. Comput. Methods Appl. Mech. Eng. 376, 113620 (2021)
- Boccaletti, S., Kurths, J., Osipov, G., Valladares, D., Zhou,
 C.: The synchronization of chaotic systems. Phys. Rep. 366(1–2), 1 (2002)
- Rybin, V., Tutueva, A., Karimov, T., Kolev, G., Butusov, D., Rodionova, E.: Optimizing the synchronization parameters in adaptive models of Rössler system. In: 2021 10th Mediterranean Conference on Embedded Computing (MECO). IEEE, pp. 1–4 (2021)
- Karimov, T., Rybin, V., Kolev, G., Rodionova, E., Butusov,
 D.: Chaotic communication system with symmetry-based modulation. Appl. Sci. 11(8), 3698 (2021)
- Wanner, G., Hairer, E.: Solving Ordinary Differential Equations II, vol. 375. Springer, Berlin, Heidelberg, New York (1996)
- Ricci, L., Perinelli, A., Castelluzzo, M., Euzzor, S., Meucci,
 R.: Experimental evidence of chaos generated by a minimal universal oscillator model. Int. J. Bifurc. Chaos 31(12), 2150205 (2021)
- Myasin, E., Kotov, V.: Effect of a low-frequency noise signal on the supply circuit of the millimeter-band generator of single-frequency and chaotic oscillations designed on an avalanche transit-time diode. J. Commun. Technol. Electron. 63(10), 1191 (2018)

Publisher's Note Springer Nature remains neutral with regard to jurisdictional claims in published maps and institutional affiliations.

Springer Nature or its licensor holds exclusive rights to this article under a publishing agreement with the author(s) or other rightsholder(s); author self-archiving of the accepted manuscript version of this article is solely governed by the terms of such publishing agreement and applicable law.

